Low-noise high-gain large-bandwidth transimpedance amplifier with cascode-type preamplifier for cryogenic STM

Ying-Xin Liang

Sch Phys & Elect Engn, Anyang Normal Univ, No.436, Xiange Avenue, Anyang, 455000, Henan, China.

Contributing authors: cryoliang@qq.com;

Abstract

A low-noise high-gain large-bandwidth transimpedance amplifier (TIA) for cryogenic scanning tunneling microscope (CryoSTM) is proposed. The TIA connected with the tip-sample component in CryoSTM is called as CryoSTM-TIA. The CryoSTM-TIA has a transimpedance gain of 10 G$\mathbf{\Omega}$, a bandwidth of over 100 kHz, and an equivalent input noise current power spectral density less than 4 $\mathbf{(fA)^2/Hz}$ at 100 kHz. The low inherent noise of the CryoSTM-TIA is due to its special design: (1) its pre-amplifier (Pre-Amp) is made of the low-noise cryogenic high electron mobility transistors; (2) the cascode-type configuration for the Pre-Amp is used to avoid Miller effect to reduce its input capacitance $\boldsymbol{C}_{\mathrm{A}}$; (3) the capacitance of the cable connected the Pre-Amp input to the tip, i.e. $\boldsymbol{C}_{\mathrm{I}}$, is minimized; (4) thermal noise sources, such as the feedback resistor, are placed in the cryogenic zone. Its high gain and large-bandwidth are realized together, due to the application of the frequency compensation in the feedback loop, the reduced $\boldsymbol{C}_{\mathrm{A}}$, and the minimized $\boldsymbol{C}_{\mathrm{I}}$. This apparatus can be used for fast high-energy-resolution measurements of scanning tunneling spectra for low conductivity materials, especially for measuring their scanning tunneling shot noise spectra.

Keywords: Cryogenic scanning tunneling microscope, Transimpedance amplifier, High electron mobility transistor, Equivalent input noise current power spectral density, Scanning tunneling shot noise spectra

1 Introduction

High performance transimpedance amplifier (TIA) for cryogenic scanning tunneling microscope (CryoSTM) is a key element in scanning tunneling microscopy/spectroscopy [1–3]. For the application of the STM for more complex organic systems, such as biological macromolecules and membranes, the main problems are the ability for the biological samples to sustain only an extremely low current [4]. And, for low-conductivity materials, such as wide bandgap semiconductors, the tunnel current is typically less than 100 pA [5]. Therefore, the low-noise high-gain TIA is needed for these works. For the existing TIAs with the gain higher than 1 GΩ, the typical bandwidth is only several kHz [6, 7], which is too low for some applications, such as the shot noise measurements [8]. And, the inherent noise of these high gain TIA are quite large [4–7].

In this work, the CryoSTM-TIA with the transimpedance gain of 10 GΩ and bandwidth higher than 100 kHz is proposed. Its inherent noise is only 0.21 $(\text{fA})^2/\text{Hz}$ at 10 kHz, and 3.1 $(\text{fA})^2/\text{Hz}$ at 100 kHz. And, its transient response time is less than 10 μs. For low-conductivity materials, with this apparatus, fast high-energy-resolution scanning tunneling spectra (STS) measurements can be performed and very low tunneling shot noise of quantum systems can be measured.

2 Circuit of the proposed CryoSTM-TIA

Fig.1 shows the circuit of the proposed CryoSTM-TIA. It consists of four components: the pre-amplifier (Pre-Amp) shown in dashed box (a1) and dashed box (a2) of Fig.1, the post-amplifier (Post-Amp) shown in dashed box (b), the compensated feedback network shown in dashed box (c), and the signal source circuit shown in dashed box (d). The two stage amplifier made of the Pre-Amp and Post-Amp is called as Macro operational amplifier (OPA), denoted as Macro-OPA. The Macro-OPA is connected with the feedback network to form the TIA. The components placed in the cryogenic zone are shown in the dotted box, and all of them are discrete ones. The parameters of all components of the CryoSTM-TIA circuit are listed in Table 1. The total power consumption of the cryogenic stage of the circuit is no more than 2.5 mW, according to Table 1.

2.1 Design of Pre-Amp

The differential amplifier part of the Pre-Amp is shown in dashed box (a1) of Fig.1. The transistors $H1_1$, $H2_1$, $H1_2$, and $H2_2$ are cryogenic high electron mobility transistors (HEMTs), i.e. CNRS-HEMTs developed by CNRS/LPN in France [9, 10]. The CNRS-HEMT is able to operate at the cryogenic zone below 0.5 K, and its power is only 0.1 mW. Its parameters are listed in Table 1, where $\overline{e_{\text{H}}^2}$ is the equivalent input noise voltage PSD of CNRS-HEMT, and $\overline{i_{\text{H}}^2}$ is its equivalent input noise current PSD [10]. The 4 CNRS-HEMTs are

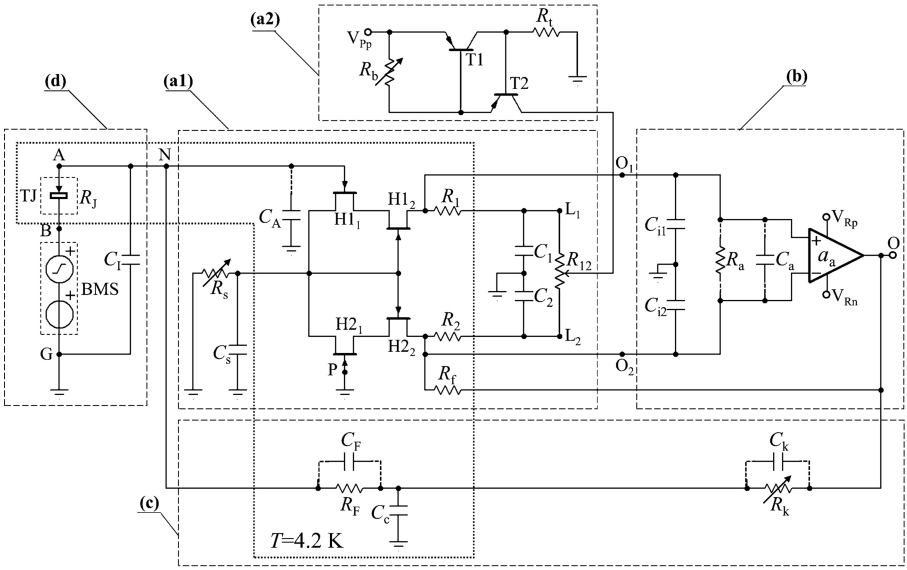

Fig. 1 Circuit of the proposed CryoSTM-TIA. Differential amplifier part of Pre-Amp is shown in dashed box (a1), constant-current source part of Pre-Amp in dashed box (a2), the Post-Amp in dashed box (b), the compensated feedback network in dashed box (c), and the signal source circuit in dashed box (d). The components placed in the cryogenic zone are shown in the dotted box. The parameters of all components of CryoSTM-TIA circuit are listed in Table 1.

identical [11]. A cascode-type configuration for the Pre-Amp composed of CNRS-HEMTs $H1_1$, $H2_1$, $H1_2$, and $H2_2$ is used. The sources of $H1_1$ and $H2_1$ are connected together and grounded via a variable resistor R_s. The drains of $H1_2$ and $H2_2$ are connected to R_1 and R_2 respectively, and $R_1 = R_2 = R_L$. R_{12} is a potentiometer, and $R_{12} \leq 0.02R_L$. The movable terminal of R_{12} is connected to the output of the constant-current source, $R_{L1} = R_1 + \lambda R_{12}$ and $R_{L2} = R_2 + (1 - \lambda)R_{12}$, and λ can vary from 0 to 1. Gate N of $H1_1$ as the input of the Pre-Amp is connected to the tip of the CryoSTM, and gate P of $H2_1$ is connected to ground permanently. C_A is the input capacitance of the Pre-Amp. C_s, C_1 and C_2 as the AC short circuit capacitors are 0.1 mF. $H1_1$, $H2_1$, $H1_2$, $H2_2$, R_1, and R_2 are placed in the cryogenic zone. $H1_1$ is placed as close as possible to the tip of the CryoSTM, so the capacitance of the cable connected gate N of $H1_1$ to the tip, denoted as C_I, is reduced to less than 0.5 pF.

In this work, the voltage difference between inputs P and N of the Pre-Amp is called the differential input voltage of the Pre-Amp, and the voltage difference between outputs O_1 and O_2 is the differential output voltage of the Pre-Amp. The ratio between its AC differential output voltage and AC input voltage is the voltage gain of the Pre-Amp A_{vP}. Since the gain-bandwidth-product of the CNRS-HEMT is $g_m/[2\pi(C_{gs} + C_{gd})] \approx 1$ GHz, the bandwidth of the Pre-Amp is not less than 25 MHz [3, 10]. A cascode-type configuration

Table 1 Parameters of all components of CryoSTM-TIA circuit

CNRS-HEMTs $H1_1$, $H1_2$, $H2_1$, $H2_2$			
Gate–source resistance R_A			>10 TΩ
Transconductance g_m			40 mS
Channel conductance g_d			1 mS
Gate–source capacitance C_{gs}			5 pF
Gate–drain capacitance C_{gd}			1 pF
Drain–source voltage V_{ds}			100 mV
Drain–source current I_{ds}			1 mA
$\overline{e_H^2}$ ((nV)^2/Hz)		10 kHz	0.25
		100 kHz	0.07
$\overline{i_H^2}$ ((fA)^2/Hz)		10 kHz	0.1
		100 kHz	1
Pre-Amp			
R_L	1 kΩ	R_{12}	20 Ω
R_s	50 ± 2 Ω	C_s	0.1 mF
C_1, C_2	0.1, 0.1 mF		
T_1 & T_2	BJT BFT93 [12]	R_b	347 ± 1 Ω
R_t	20 kΩ	V_{Pp}	+12 V
Post-Amp			
Rear-OPA		THS4021	
a_{a0}	97.5 dB	f_b	14.5 kHz
C_a	1.5 pF	R_a	1 MΩ
Supply voltages V_{Rp}, V_{Rn}		+15, -15 V	
R_f	1.5 MΩ	C_i	100 pF
Feedback network			
R_F	10 GΩ	C_F	0.3 pF
R_k	500 kΩ	C_k	0.2 pF
C_c	6 nF		
Signal source circuit			
R_J	≥10 MΩ	C_I	0.5 pF

Note: ± indicates the variable resistance range. Without specification, the default value after ± is 0.

for the Pre-Amp of the CryoSTM-TIA is used to avoid Miller effect, so that the gain is increased and the input capacitance is reduced, comparing to those in Ref.[3]. In (0, 3 MHz], A_{vP} can be considered as a constant,

$$A_{vP} = g_m R_L, \tag{2.1}$$

i.e. $A_{vP} = 40$. The input capacitance of the Pre-Amp is

$$C_A = C_{gs} + (2 + g_d R_L) C_{gd}. \tag{2.2}$$

i.e. $C_A = 8$ pF. The input resistance of the Pre-Amp R_A is the gate-source resistance of the CNRS-HEMT, and it is about $10 \sim 100$ TΩ, so it can be considered as infinity.

The dashed box (a2) of Fig.1 shows the constant-current source part of the Pre-Amp that is the same as that in Ref. [3]. For a given resistance R_b, there are nearly no fluctuations for the current I_{sour} generated by the constant-current

source, even though the voltage V_{Pp} of the positive voltage source fluctuates greatly, which ensures the stability of the static operating points of $\mathrm{H1}_1$, $\mathrm{H2}_1$, $\mathrm{H1}_2$, and $\mathrm{H2}_2$ [3].

2.2 Design of Post-Amp and composition of Macro-OPA

The Post-Amp circuit is shown in the dashed box (b) of Fig.1, and its parameters are listed in Table 1. There is a commercial OPA in the circuit, called as Rear-OPA, which is THS4021 [13] in this work. And, its open loop voltage gain a_{a} can be approximately expressed as $a_{\mathrm{a}} = a_{\mathrm{a0}}/(1 + jf/f_{\mathrm{b}})$, where f_{b} is its upper cut-off frequency. R_{a} and C_{a} are the input resistance and capacitance of the Rear-OPA respectively. The feedback resistor R_{f} is connected to the output of the Rear-OPA and its inverting input. R_{f} is 1.5 MΩ. There are two cables in the Post-Amp, connecting outputs of the Pre-Amp O_1 and O_2 to the non-inverting input and inverting input of the Rear-OPA respectively. The capacitance of the two cables is C_{i1} and C_{i2} respectively, and $C_{\mathrm{i1}} = C_{\mathrm{i2}} = C_{\mathrm{i}} \approx 100$ pF. In this work, $C_{\mathrm{i}} >> C_{\mathrm{a}}$. Cascade the Pre-Amp and Post-Amp to form the Macro-OPA. The voltage gain of the Macro-OPA $a_{\mathrm{A}}(f)$ is the ratio between the AC voltage at the output and the AC voltage at the input. When $f \to 0$, $a_{\mathrm{A}} \to a_{\mathrm{A0}}$. a_{A0} is the DC voltage gain of the Macro-OPA. And, The voltage gain of the Macro-OPA $a_{\mathrm{A}}(f)$ can be expressed as

$$a_{\mathrm{A}} = A_{\mathrm{vP}} A_{\mathrm{vR}}. \tag{2.3}$$

By the nodal analysis method, a_{A} can be obtained. And then, with A_{vP} expressed by Eq.(2.1), A_{vR} can be obtained by Eq.(2.3). In $f \leq 3$ MHz,

$$A_{\mathrm{vR}} \approx \frac{R_{\mathrm{f}}}{R_{\mathrm{L}}} \cdot \frac{1}{1 + \frac{R_{\mathrm{f}}}{a_{\mathrm{a}} R_{\mathrm{L}}} + j2\pi f \frac{R_{\mathrm{f}} C_{\mathrm{i}}}{a_{\mathrm{a}}}}. \tag{2.4}$$

The simulation results of a_{A} are shown in Fig.2(a), and the upper cut-off frequency of a_{A} is about 1.26 MHz.

2.3 Frequency compensation of feedback loop

In order to increase the bandwidth of the CryoSTM-TIA, for the high feedback resistor R_{F} with parasitic capacitance C_{F}, frequency compensation must be used in feedback loop. In Fig.1, the compensated feedback network is shown in the dashed box (c). Taking C_{c} equal to kC_{F}, where k is above 10^4, adjust R_{k} equal to R_{F}/k, realizing $R_{\mathrm{k}} C_{\mathrm{c}} = R_{\mathrm{F}} C_{\mathrm{F}}$ [3, 14]. The output voltage of the TIA as $\dot{V}_{\mathrm{o}}$ generates the current $\dot{I}_{\mathrm{F}}$ flowing to the TIA input N, so

$$Z_{\mathrm{F}}(f) = \frac{\dot{V}_{\mathrm{o}}}{\dot{I}_{\mathrm{F}}} \approx \frac{R_{\mathrm{k}} + R_{\mathrm{F}}}{1 + j2\pi f R_{\mathrm{k}} C_{\mathrm{k}}} \approx \frac{R_{\mathrm{F}}}{1 + j2\pi f R_{\mathrm{k}} C_{\mathrm{k}}},$$

where C_{k} is the parasitic capacitance of R_{k} [3]. $Z_{\mathrm{F}}(f)$ can be considered as the impedance of the feedback network. In $(0, 200$ kHz$]$, with the parameters of the

feedback network listed in Table 1, $|Z_F(f)| \approx R_F/|1+j2\pi f R_k C_k| > R_F/1.007$ and $|Z_F(f)| \leq R_F$, so it can be considered that $Z_F(f)$ is equal to R_F.

2.4 Circuit stability of the proposed CryoSTM-TIA

In Fig.1, the signal source circuit is shown in the dashed box (d), and its parameters are shown in Table 1. The differential resistance of the tip-sample tunnel junction (TJ) in CryoSTM is R_J, which is limited to no less than $10^{-3}R_F$ in this work. The capacitance of TJ is C_J, which is in parallel with R_J. And, C_J is estimated as several fF [3]. $C = C_A + C_I + C_J$ in this work. C_J is at least two orders of magnitude less than $C_A + C_I$, so it can be ignored in C and $C \approx C_A + C_I$. In Fig.1, the source BMS provides the DC bias V_i and sinusoidal modulated signal voltage $\dot{V}_i$ for the CryoSTM-TIA. In the following simulation, C_I is always taken as 0.5 pF. The TIA connects the signal source circuit to form the CryoSTM-TIA. According to the circuit parameters in Table 1, the performances of the CryoSTM-TIA can be simulated by TINA-TI [15].

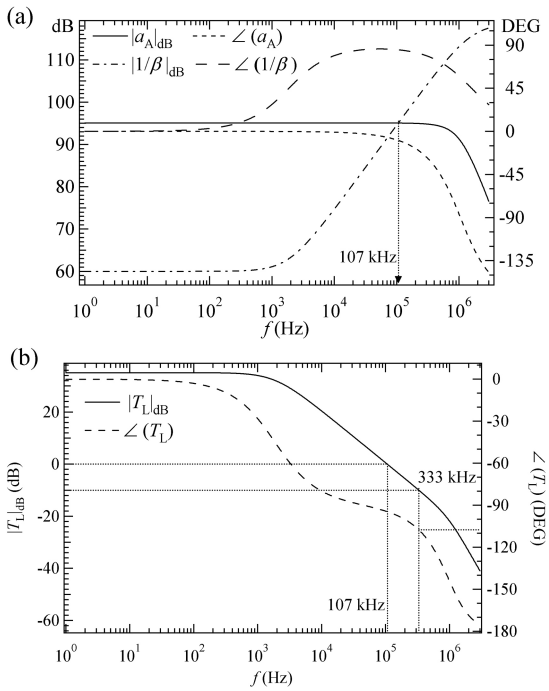

Fig. 2 (a) TINA-TI simulation results for the voltage gain a_A of the Macro-OPA and $1/\beta(f)$ with $R_J = 10$ MΩ. $|a_A| = |1/\beta|$ at 107 kHz. (b) TINA-TI simulation results for the loop-gain T_L of the CryoSTM-TIA. $|T_L|_{dB} = 0$ at 107 kHz. Both figures show $|T_L|_{dB} = |a_A|_{dB} - |1/\beta(f)|_{dB} \leq -10$ dB in $f \geq 333$ kHz and $\angle(T_L) = \angle(a_A) - \angle(1/\beta) > -107.6°$ in $f < 333$ kHz. Hence, the CryoSTM-TIA is stable enough.

The loop gain T_{L} of the proposed CryoSTM-TIA [16] is

$$T_{\mathrm{L}}(f) = a_{\mathrm{A}}(f)\beta(f) = a_{\mathrm{A}}(f)/[1/\beta(f)], \tag{2.5}$$

in which $\beta(f)$ is the feedback factor, and its reciprocal is,

$$1/\beta(f) \approx 1 + Z_{\mathrm{F}}[1/R_{\mathrm{J}} + 1/R_{\mathrm{A}} + j2\pi f(C_{\mathrm{A}} + C_{\mathrm{I}})]. \tag{2.6}$$

For the Macro-OPA, Fig.2(a) shows the curves for $|a_{\mathrm{A}}(f)|_{\mathrm{dB}}$ and $\angle(a_{\mathrm{A}}(f))$ simulated by TINA-TI and the calculated results of $|1/\beta(f)|_{\mathrm{dB}}$ and $\angle(1/\beta(f))$ with $R_{\mathrm{J}} = 10$ MΩ by Eq.(2.6). Fig.2(b) shows the corresponding $|T_{\mathrm{L}}(f)|_{\mathrm{dB}}$ and $\angle(T_{\mathrm{L}}(f))$. Both figures show $|T_{\mathrm{L}}|_{\mathrm{dB}} = |a_{\mathrm{A}}|_{\mathrm{dB}} - |1/\beta(f)|_{\mathrm{dB}} \leq -10$ dB in $f \geq 333$ kHz and $\angle(T_{\mathrm{L}}) = \angle(a_{\mathrm{A}}) - \angle(1/\beta) > -107.6°$ in $f < 333$ kHz. The CryoSTM-TIA is stable with gain margin more than 10 dB and phase margin more than 82°. It is easy to prove that the circuit is stable with $R_{\mathrm{J}} > 10$ MΩ.

2.5 Voltage gain and transimpedance gain of the proposed CryoSTM-TIA

With the frequency compensation as mentioned in Section 2.3, it can be considered that Z_{F} is equal to R_{F} in $(0, 200$ kHz$]$. Considering the TJ capacitance C_{J}, the TJ impedance should be $Z_{\mathrm{J}} = R_{\mathrm{J}}/(1+j2\pi f R_{\mathrm{J}} C_{\mathrm{J}})$. And, $C \approx C_{\mathrm{A}} + C_{\mathrm{I}}$. As the AC input voltage $\dot{V}_{\mathrm{i}}$ is applied by BMS, the output voltage of the CryoSTM-TIA is $\dot{V}_{\mathrm{o}}$, and the voltage gain of the CryoSTM-TIA is $A_{\mathrm{v}} = \dot{V}_{\mathrm{o}}/\dot{V}_{\mathrm{i}}$. By the node analysis method, in $(0, 200$ kHz$]$, A_{v} is

$$A_{\mathrm{v}} \approx -\frac{R_{\mathrm{F}}}{Z_{\mathrm{J}}} \cdot \frac{1}{1 + \frac{1}{a_{\mathrm{A}}} + \frac{R_{\mathrm{F}}}{a_{\mathrm{A}} R_{\mathrm{J}}} + \frac{R_{\mathrm{F}}}{a_{\mathrm{A}} R_{\mathrm{A}}} + j2\pi f \frac{R_{\mathrm{F}}(C_{\mathrm{A}}+C_{\mathrm{I}})}{a_{\mathrm{A}}}}. \tag{2.7}$$

Setting $\dot{V}_{\mathrm{i}} = 0$ and applying a sinusoidal current source $\dot{I}_{\mathrm{i}}$ in parallel with TJ, the output voltage $\dot{V}_{\mathrm{o}}$ is generated at the output of the CryoSTM-TIA. $A_{\mathrm{i}} = \dot{V}_{\mathrm{o}}/\dot{I}_{\mathrm{i}}$ is called as the transimpedance gain of the CryoSTM-TIA. In $(0, 200$ kHz$]$, A_{i} is

$$A_{\mathrm{i}} \approx -\frac{R_{\mathrm{F}}}{1 + \frac{1}{a_{\mathrm{A}}} + \frac{R_{\mathrm{F}}}{a_{\mathrm{A}} R_{\mathrm{J}}} + \frac{R_{\mathrm{F}}}{a_{\mathrm{A}} R_{\mathrm{A}}} + j2\pi f \frac{R_{\mathrm{F}}(C_{\mathrm{A}}+C_{\mathrm{I}})}{a_{\mathrm{A}}}}. \tag{2.8}$$

Fig.2(a) shows $|1/\beta| = |a_{\mathrm{A}}|$ (i.e.$|T_{\mathrm{L}}|_{\mathrm{dB}} = 0$) at 107 kHz, which is much smaller than the upper cut-off frequency of a_{A} as 1.26 MHz. According to Eq.(2.8), the upper cut-off frequency of the CryoSTM-TIA f_{hCST}, i.e. its -3 dB frequency, should be $f_{\mathrm{hCST}} \approx |a_{\mathrm{A0}}|/[2\pi R_{\mathrm{F}}(C_{\mathrm{A}} + C_{\mathrm{I}})]$. Therefore, f_{hCST} should be at the frequency about where $|a_{\mathrm{A}}| = |1/\beta|$, i.e. 107 kHz. By using the cascode-type configuration in the Pre-Amp, Miller effect is avoided, so C_{A} is only 8 pF. Therefore, f_{hCST} can be higher than 100 kHz with R_{F} of 10 GΩ.

Disconnecting the TIA with the signal source circuit, and applying a sinusoidal current source $\dot{I}_{\mathrm{iT}}$ into the input of the TIA, the output voltage

$\dot{V}_{\rm oT}$ is generated at the output of the TIA. $A_{\rm iT} = \dot{V}_{\rm oT}/\dot{I}_{\rm iT}$ is called as the transimpedance gain of the TIA. In $(0, 200\ \text{kHz}]$, $A_{\rm iT}$ is

$$A_{\rm iT} = -\frac{R_{\rm F}}{1 + \frac{1}{a_{\rm A}} + \frac{R_{\rm F}}{a_{\rm A} R_{\rm A}} + j2\pi f \frac{R_{\rm F} C_{\rm A}}{a_{\rm A}}}, \tag{2.9}$$

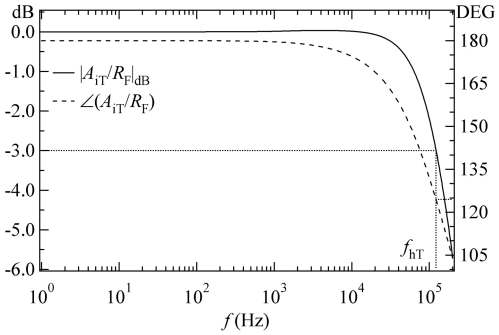

Fig. 3 TINA-TI simulation results for $A_{\rm iT}/R_{\rm F}$, $A_{\rm iT}$ is the transimpedance gain of the TIA in the proposed CryoSTM-TIA. $|A_{\rm iT}(f_{\rm hT})/R_{\rm F}|_{\rm dB} = -3$ dB and $\angle(A_{\rm iT}(f_{\rm hT})/R_{\rm F}) = 124.5°$ at $f_{\rm hT} = 122$ kHz.

Fig.3 shows $A_{\rm iT}/R_{\rm F}$ simulated by TINA-TI. The simulation results show that its -3 dB frequency is $f_{\rm hT} = 122$ kHz. The simulation results are consistent with the calculated results by (2.1), (2.3), (2.4), and (2.9). In addition, it is found that $|A_{\rm iT}(f)/R_{\rm F}|_{\rm dB}$ decreases monotonically, and there is no "gain peaking" on the curve, which also indicates the circuit is quite stable [16]. Comparing Eqs.(2.8) and (2.9), as $C_{\rm A} + C_{\rm I} \approx C_{\rm A}$, $f_{\rm hCST} \approx 107$ kHz for $R_{\rm J} = 10$ MΩ is approximately equal to $f_{\rm hT}$, but a little smaller than it.

2.6 Transient response of the proposed CryoSTM-TIA

For the CryoSTM-TIA, the time taken from adding the input step signal voltage to the output response stably within 0.1% error is called transient response time $t_{\rm r}$, which is less than 10 μs as shown in Fig.4. There is no "ringing" and "overshoot" characteristics in the output response curve, indicating the circuit stability [16].

Since $t_{\rm r} < 10$ μs, the time delay of the voltage rise/fall step for STS measurements only depends the limit of the source meter, which is about 0.1 ms [17]. The frequency of the modulated signal for STS measurements with this apparatus is capable as high as 100 kHz due to the large-bandwidth of the CryoSTM-TIA. Therefore, fast STS measurements are capable to be performed with this apparatus.

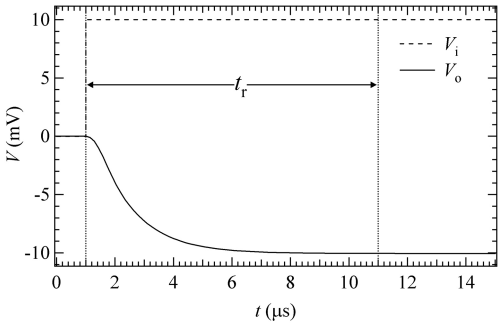

Fig. 4 TINA-TI simulation results for the transient response of the proposed CryoSTM-TIA, as $R_J = R_F$. The dashed curve is the step input signal V_i and solid curve is the output response V_o. Transient response time $t_r < 10$ μs.

3 Inherent noise of the proposed CryoSTM-TIA

3.1 Noise model of CryoSTM-TIA

The equivalent input noise voltage of the OPA is denoted as e_A and its equivalent input noise current is i_A, and their harmonic components at frequency f are E_A and I_A respectively. By Wiener-Khintchine theorem, $\begin{pmatrix} \overline{e_A^2} & \overline{e_A i_A^*} \\ \overline{i_A e_A^*} & \overline{i_A^2} \end{pmatrix}$ can be obtained from $\begin{pmatrix} E_A E_A^* & E_A I_A^* \\ I_A E_A^* & I_A I_A^* \end{pmatrix}$ [18, 19]. For the former matrix, the two matrix elements on the main diagonal are the equivalent input noise voltage PSD of the OPA and its equivalent input noise current PSD. The two matrix elements on the sub-diagonal are its equivalent input noise voltage-current PSD and equivalent input noise current-voltage PSD.

The equivalent input noise voltage of the TIA is denoted as e_T and its equivalent input noise current is i_T, and their harmonic components at f are E_T and I_T respectively. The noise voltage of the feedback resistor R_F is denoted as e_F and its harmonic component at f is E_F.

For the TIA, the circuit containing all noise sources with the input short-circuit is shown as Fig.5(a), and the output noise voltage is e_{oTv}. The noiseless circuit with the equivalent input noise voltage of the TIA e_T as the input signal is shown as Fig.5(b), and its harmonic component at frequency f is E_T. And, the output noise voltage is e_{oTve}. For calculating e_T, the equations are established on the equivalency of the above two circuits, i.e. $e_{oTv} = e_{oTve}$. Therefore, by nodal analysis method,

$$E_T = E_A. \tag{3.1}$$

For the TIA, the circuit containing all noise sources with the input open-circuit is shown as Fig.6(a), and the output noise voltage is e_{oTi}. The noiseless circuit with the equivalent input noise current of the TIA i_T as the input

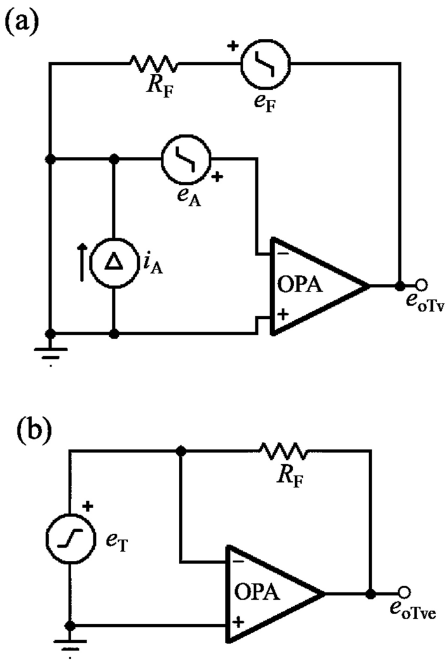

Fig. 5 (a) TIA circuit with the input short-circuit containing the equivalent input noise voltage of OPA e_A and its equivalent input noise current i_A, and the output noise voltage of e_{oTv}; (b) Noiseless TIA circuit with the equivalent input noise voltage of the TIA e_T as the input signal, and the output noise voltage of e_{oTve}; the equivalency of the above two circuits means $e_{oTv} = e_{oTve}$.

signal is shown as Fig.6(b), and its harmonic component at frequency f is I_T. And, the output noise voltage is e_{oTie}. For calculating i_T, the equations are established on the equivalency of the above two circuits, i.e. $e_{oTi} = e_{oTie}$. Therefore, by the nodal analysis method,

$$I_T = I_A + (E_A + E_F)/R_F. \tag{3.2}$$

By Wiener-Khintchine theorem, $\begin{pmatrix} \overline{e_T^2} & \overline{e_T i_T^*} \\ \overline{i_T e_T^*} & \overline{i_T^2} \end{pmatrix}$ can be obtained from $\begin{pmatrix} E_T E_T^* & E_T I_T^* \\ I_T E_T^* & I_T I_T^* \end{pmatrix}$. For the former matrix, the two matrix elements on the main diagonal are the equivalent input noise voltage PSD of the TIA and its equivalent input noise current PSD. The two matrix elements on the sub-diagonal are its equivalent input noise voltage-current PSD and equivalent input noise current-voltage PSD. The temperature of R_F is T, and the thermal noise voltage PSD of R_F is $\overline{e_F^2} = 4k_B T R_F$. $\overline{e_T^2}$, $\overline{i_T^2}$, $\overline{e_T i_T^*}$, and $\overline{i_T e_T^*}$ can be expressed

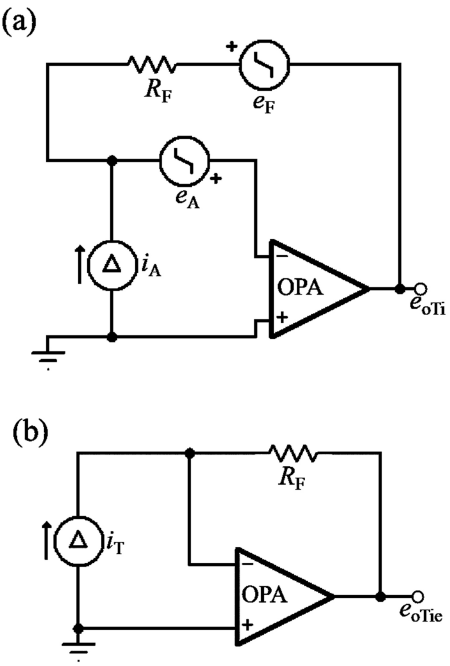

Fig. 6 (a) TIA circuit with the input open-circuit containing the equivalent input noise voltage of OPA e_A and its equivalent input noise current i_A, and the output noise voltage of e_{oTi}; (b) Noiseless TIA circuit with the equivalent input noise current of the TIA i_T as the input signal, and the output noise voltage of e_{oTie}; the equivalency of the above two circuits means $e_{oTi} = e_{oTie}$.

as

$$\overline{e_T^2} = \overline{e_A^2}, \tag{3.3}$$

$$\overline{i_T^2} = \overline{i_A^2} + \overline{e_A^2}/R_F^2 + 4k_BT/R_F, \tag{3.4}$$

$$\overline{e_T i_T^*} = (\overline{i_T e_T^*})^* = \overline{e_A i_A^*} + \overline{e_A^2}/R_F. \tag{3.5}$$

The TIA connected with the tip-sample component in STM is called as STM-TIA. For the STM-TIA, the circuit containing the TIA noise sources is shown as Fig.7(a), and the output noise voltage is e_o. The noiseless circuit with the equivalent input noise current of the TIA i_{in} as the input signal is shown as Fig.7(b), and its harmonic component at frequency f is I_{in}. And, the output noise voltage is e_{oe}. For calculating the equivalent input noise current of the STM-TIA, the equations are established on the equivalency of the above two circuits, i.e. $e_o = e_{oe}$. Therefore, by the nodal analysis method,

$$I_{in} = I_T + (1/R_J + j2\pi f C_{IJ})\, E_T. \tag{3.6}$$

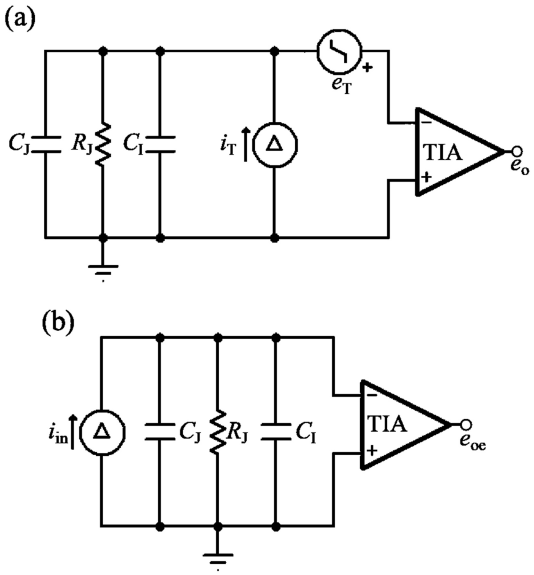

Fig. 7 (a) STM-TIA circuit containing the equivalent input noise voltage of TIA e_T and its equivalent input noise current i_T, and the output noise voltage of e_o; (b) Noiseless STM-TIA circuit with the equivalent input noise current i_{in} as the input signal, and the output noise voltage of e_{oe}; the equivalency of the above two circuits means $e_o = e_{oe}$.

In this work, $C_{IJ} = C_I + C_J$. $\overline{i_{in}^2}$ can be obtained from $I_{in}I_{in}^*$ by Wiener-Khintchine theorem. The equivalent input noise current PSD of the CryoSTM-TIA $\overline{i_{in}^2}$ is

$$\begin{aligned}\overline{i_{in}^2} =&\overline{i_T^2} + \left(\frac{1}{R_J^2} + (2\pi f)^2 C_{IJ}^2\right)\overline{e_T^2} \\ &+ \left(\frac{1}{R_J} + j2\pi f C_{IJ}\right)\overline{e_T i_T^*} + \left(\frac{1}{R_J} - j2\pi f C_{IJ}\right)\overline{i_T e_T^*}. \end{aligned} \tag{3.7}$$

Putting Eqs.(3.3)-(3.5) into Eq.(3.7),

$$\begin{aligned}\overline{i_{in}^2} =&\overline{i_A^2} + \frac{4k_B T}{R_F} + \left[\frac{1}{R_J^2} + \frac{1}{R_F^2} + (2\pi f)^2 C_{IJ}^2\right]\overline{e_A^2} \\ &+ \left(\frac{1}{R_J} + j2\pi f C_{IJ}\right)\left(\overline{e_A i_A^*} + \frac{\overline{e_A^2}}{R_F}\right) + \left(\frac{1}{R_J} - j2\pi f C_{IJ}\right)\left(\overline{i_A e_A^*} + \frac{\overline{e_A^2}}{R_F}\right). \end{aligned} \tag{3.8}$$

3.2 Equivalent input voltage noise and equivalent input current noise of Macro-OPA

For the circuit of the proposed CryoSTM-TIA shown in Fig.1, the differential equivalent circuit with all noise sources is used to calculate its equivalent input noise.

The equivalent input noise voltage and equivalent input noise current of $H1_1$ are denoted as e_{11} and i_{11} respectively, and their harmonic components at frequency f are E_{11} and I_{11} respectively. For $H2_1$, $H1_2$, and $H2_2$, there are e_{21}, e_{12}, e_{22}, i_{21}, i_{12}, i_{22}, E_{21}, E_{12}, E_{22}, I_{21}, I_{12}, and I_{22}. The resistors R_1, R_2, and R_f are in the cryogenic zone of 4.2 K. The noise voltages generated by R_1, R_2, and R_f are e_1, e_2, and e_f respectively, and their harmonic components at frequency f are E_1, E_2, and E_f respectively. The equivalent input noise voltage and equivalent input noise current of Rear-OPA are denoted as e_a and i_a respectively, and their harmonic components at frequency f are E_a and I_a respectively. These noise sources are independent.

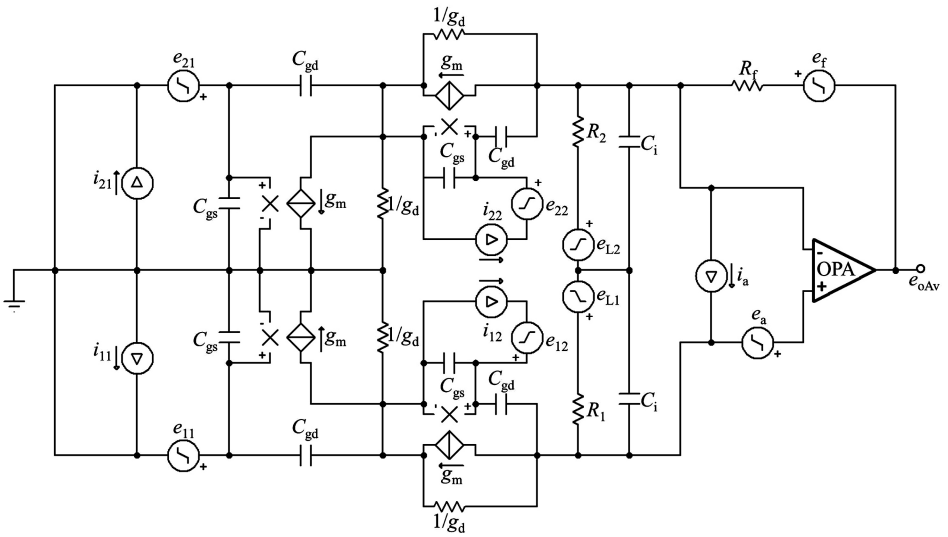

Fig. 8 Macro-OPA circuit with the input short-circuit containing all noise sources, and the output noise voltage of e_{oAv}.

For the Macro-OPA, the circuit containing all noise sources with the input short-circuit is shown as Fig.8, and the output noise voltage is e_{oAv}. The noiseless circuit with the equivalent input noise voltage of the Macro-OPA e_A as the input signal is shown as Fig.9, and its harmonic component at frequency f is E_T. And, the output noise voltage is e_{oAve}. For calculating e_A, the equations are established on the equivalency of the above two circuits, i.e.

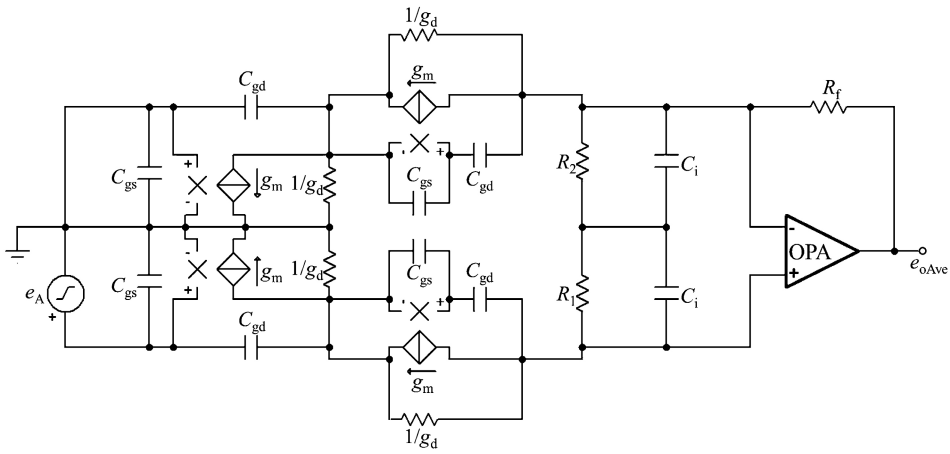

Fig. 9 Noiseless Macro-OPA with the equivalent input noise voltage e_{A} as the input signal, and the output noise voltage of e_{oAve}.

$e_{\mathrm{oAv}} = e_{\mathrm{oAve}}$. Therefore, by nodal analysis method,

$$E_{\mathrm{A}} \approx E_{11} - E_{21} + \frac{g_{\mathrm{d}}}{g_{\mathrm{m}}}(E_{12} - E_{22}) + \frac{I_{12} - I_{22}}{g_{\mathrm{m}}} + \frac{E_1 - E_2}{g_{\mathrm{m}} R_{\mathrm{L}}} - \frac{E_{\mathrm{f}}}{g_{\mathrm{m}} R_{\mathrm{f}}} - \frac{E_{\mathrm{A}}}{g_{\mathrm{m}} R_{\mathrm{L}}} - \frac{2I_{\mathrm{A}}}{g_{\mathrm{m}}} \tag{3.9}$$

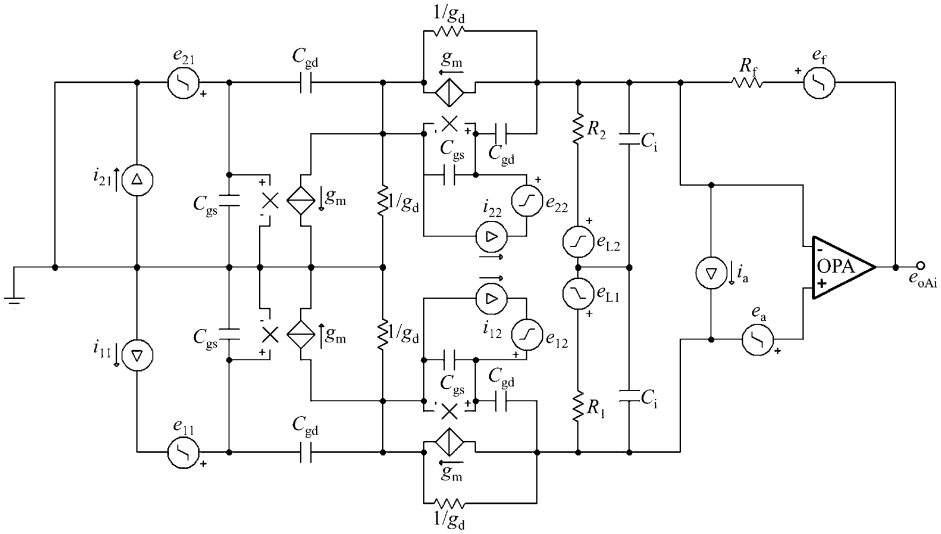

Fig. 10 Macro-OPA circuit with the input open-circuit containing all noise sources, and the output noise voltage of e_{oAi}.

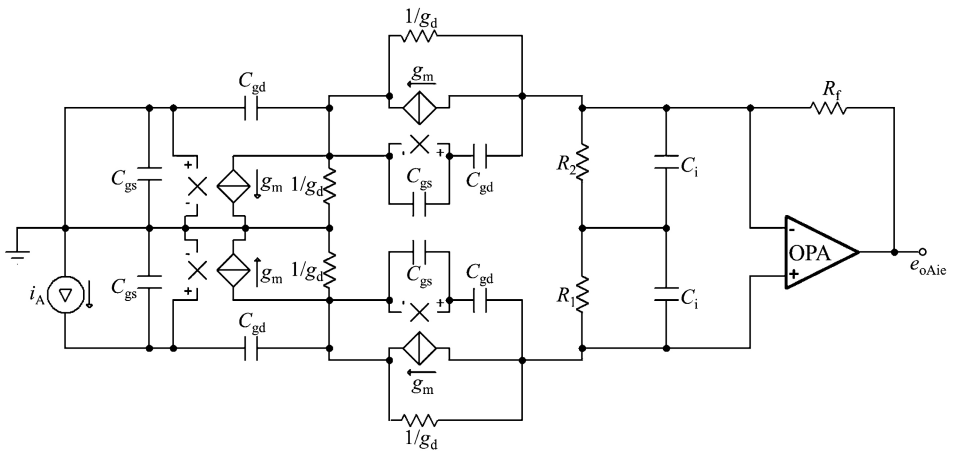

Fig. 11 Noiseless Macro-OPA with the equivalent input noise current i_{A} as the input signal, and the output noise voltage of e_{oAie}.

For the Macro-OPA, the circuit containing all noise sources with the input open-circuit is shown as Fig.10, and the output noise voltage is e_{oAi}. The noiseless circuit with the equivalent input noise current of the Macro-OPA i_{A} as the input signal is shown as Fig.11, and its harmonic component at frequency f is I_{A}. And, the output noise voltage is e_{oAie}. For calculating i_{A}, the equations are established on the equivalency of the above two circuits, i.e. $e_{\mathrm{oAi}} = e_{\mathrm{oAie}}$. Therefore, by nodal analysis method,

$$\begin{aligned} I_{\mathrm{A}} \approx & I_{11} + j2\pi f \left[\left(\frac{g_{\mathrm{d}} C_{\mathrm{gs}}}{g_{\mathrm{m}}} + C_{\mathrm{gd}} \right) E_{12} + \frac{C_{\mathrm{gs}} + C_{\mathrm{gd}}}{g_{\mathrm{m}}} I_{12} \right] \\ & - j2\pi f C_{\mathrm{A}} \left(E_{21} + \frac{g_{\mathrm{d}}}{g_{\mathrm{m}}} E_{22} + \frac{I_{22}}{g_{\mathrm{m}}} - \frac{E_2}{g_{\mathrm{m}} R_{\mathrm{L}}} - \frac{E_{\mathrm{f}}}{g_{\mathrm{m}} R_{\mathrm{f}}} \right) \\ & + j2\pi f \left[\frac{C_{\mathrm{gs}} + 2C_{\mathrm{gd}}}{g_{\mathrm{m}} R_{\mathrm{L}}} (E_1 - E_{\mathrm{A}}) - 2 \frac{C_{\mathrm{gs}} + 2C_{\mathrm{gd}}}{g_{\mathrm{m}}} I_{\mathrm{A}} \right] \end{aligned} \tag{3.10}$$

By Wiener-Khintchine theorem, $\begin{pmatrix} \overline{e_{\mathrm{A}}^2} & \overline{e_{\mathrm{A}} i_{\mathrm{A}}^*} \\ \overline{i_{\mathrm{A}} e_{\mathrm{A}}^*} & \overline{i_{\mathrm{A}}^2} \end{pmatrix}$ can be obtained from $\begin{pmatrix} E_{\mathrm{A}} E_{\mathrm{A}}^* & E_{\mathrm{A}} I_{\mathrm{A}}^* \\ I_{\mathrm{A}} E_{\mathrm{A}}^* & I_{\mathrm{A}} I_{\mathrm{A}}^* \end{pmatrix}$. The noises generated by R_1, R_2, and R_{f} in $f > 1$ kHz are thermal noise, and they can be neglected [3]. Ignoring the minor terms,

$$\overline{e_{\mathrm{A}}^2} = \overline{e_{11}^2} + \overline{e_{21}^2} + \frac{\overline{e_{\mathrm{a}}^2}}{g_{\mathrm{m}}^2 R_{\mathrm{L}}^2} + \frac{4\overline{i_{\mathrm{a}}^2}}{g_{\mathrm{m}}^2} = 2\overline{e_{\mathrm{H}}^2} + \frac{\overline{e_{\mathrm{a}}^2}}{g_{\mathrm{m}}^2 R_{\mathrm{L}}^2} + \frac{4\overline{i_{\mathrm{a}}^2}}{g_{\mathrm{m}}^2}, \tag{3.11}$$

$$\overline{i_{\mathrm{A}}^2} = \overline{i_{11}^2} + (2\pi f)^2 C_{\mathrm{A}}^2 \left(\overline{e_{21}^2} + \frac{\overline{e_{\mathrm{a}}^2}}{g_{\mathrm{m}}^2 R_{\mathrm{L}}^2} \right) + (4\pi f)^2 (C_{\mathrm{gs}} + 2C_{\mathrm{gd}})^2 \frac{\overline{i_{\mathrm{a}}^2}}{g_{\mathrm{m}}^2}$$

$$= \overline{i_{\mathrm{H}}^2} + (2\pi f)^2 C_{\mathrm{A}}^2 \left(\overline{e_{\mathrm{H}}^2} + \frac{\overline{e_{\mathrm{a}}^2}}{g_{\mathrm{m}}^2 R_{\mathrm{L}}^2} \right) + (4\pi f)^2 \left(C_{\mathrm{gs}} + 2C_{\mathrm{gd}} \right)^2 \frac{\overline{i_{\mathrm{a}}^2}}{g_{\mathrm{m}}^2}, \tag{3.12}$$

$$\begin{aligned} \overline{e_{\mathrm{A}} i_{\mathrm{A}}^*} = \left(\overline{i_{\mathrm{A}} e_{\mathrm{A}}^*}\right)^* &= -j2\pi f \left[C_{\mathrm{A}} \overline{e_{21}^2} + \left(C_{\mathrm{gs}} + 2C_{\mathrm{gd}} \right) \left(\frac{\overline{e_{\mathrm{a}}^2}}{g_{\mathrm{m}}^2 R_{\mathrm{L}}^2} + \frac{4\overline{i_{\mathrm{a}}^2}}{g_{\mathrm{m}}^2} \right) \right] \\ &= -j2\pi f \left[C_{\mathrm{A}} \overline{e_{\mathrm{H}}^2} + \left(C_{\mathrm{gs}} + 2C_{\mathrm{gd}} \right) \left(\frac{\overline{e_{\mathrm{a}}^2}}{g_{\mathrm{m}}^2 R_{\mathrm{L}}^2} + \frac{4\overline{i_{\mathrm{a}}^2}}{g_{\mathrm{m}}^2} \right) \right]. \end{aligned} \tag{3.13}$$

$\overline{e_{\mathrm{a}}^2} = 2.25\ (\mathrm{nV})^2/\mathrm{Hz}$ and $\overline{i_{\mathrm{a}}^2} = 4\ (\mathrm{pA})^2/\mathrm{Hz}$ in $f \geq 10$ kHz [13]. And, $C_{\mathrm{A}} = C_{\mathrm{gs}} + 3C_{\mathrm{gd}}$. In Eqs.(3.11)-(3.13), $\overline{e_{\mathrm{a}}^2}/(g_{\mathrm{m}}^2 R_{\mathrm{L}}^2)$ is two orders of magnitude smaller than $\overline{e_{\mathrm{H}}^2}$, and $4\overline{i_{\mathrm{a}}^2}/g_{\mathrm{m}}^2$ is one order of magnitude smaller than $\overline{e_{\mathrm{H}}^2}$. Further ignoring the minor terms in Eqs.(3.11)-(3.13),

$$\overline{e_{\mathrm{A}}^2} = 2\overline{e_{\mathrm{H}}^2}, \tag{3.14}$$

$$\overline{i_{\mathrm{A}}^2} = \overline{i_{\mathrm{H}}^2} + (2\pi f)^2 C_{\mathrm{A}}^2 \overline{e_{\mathrm{H}}^2}, \tag{3.15}$$

$$\overline{e_{\mathrm{A}} i_{\mathrm{A}}^*} = \left(\overline{i_{\mathrm{A}} e_{\mathrm{A}}^*}\right)^* = -j2\pi f C_{\mathrm{A}} \overline{e_{\mathrm{H}}^2}. \tag{3.16}$$

By using the cascode-type configuration in the Pre-Amp, Miller effect is avoided, so C_{A} is only 8 pF. Therefore, $\overline{i_{\mathrm{A}}^2}$ in this work is much lower than that in Ref.[3].

3.3 Equivalent input current noise of the proposed CryoSTM-TIA

Putting Eqs.(3.14)-(3.16) into Eq.(3.8),

$$\overline{i_{\mathrm{in}}^2} = \overline{i_{\mathrm{H}}^2} + 4k_{\mathrm{B}}T/R_{\mathrm{F}} + \left[(2\pi f)^2 \left(C^2 + C_{\mathrm{IJ}}^2 \right) 2 \left(1/R_{\mathrm{J}} + 1/R_{\mathrm{F}} \right)^2 \right] \overline{e_{\mathrm{H}}^2}, \tag{3.17}$$

i.e.

$$\overline{i_{\mathrm{in}}^2} = \overline{i_{\mathrm{A}}^2} + 4k_{\mathrm{B}}T/R_{\mathrm{F}} + (2\pi f)^2 C C_{\mathrm{IJ}} \overline{e_{\mathrm{A}}^2} + \left(1/R_{\mathrm{J}} + 1/R_{\mathrm{F}} \right)^2 \overline{e_{\mathrm{A}}^2}. \tag{3.18}$$

For the proposed CryoSTM-TIA, $R_{\mathrm{F}} = 10\ \mathrm{G\Omega}$, $C_{\mathrm{A}} = 8$ pF, $C_{\mathrm{I}} = 0.5$ pF, and $C_{\mathrm{J}} = 10$ fF. R_{F} and TJ are in the cryogenic zone at 4.2K. As $R_{\mathrm{J}} = 10\ \mathrm{M\Omega}$, $\overline{i_{\mathrm{in}}^2}$ and its four components are listed in Table 2. The noise components of the CryoSTM-TIA in Ref.[3] are also listed in Table 2. The CryoSTM-TIA proposed in this work has an equivalent input noise current PSD of 0.21 $(\mathrm{fA})^2/\mathrm{Hz}$ at 10 kHz and 3.1 $(\mathrm{fA})^2/\mathrm{Hz}$ at 100 kHz, which is much lower than that in Ref.[3].

Since the inherent noise of the CryoSTM-TIA is only 3.1 $(\mathrm{fA})^2/\mathrm{Hz}$ at 100 kHz, considering Q factor for the typical lock-in amplifier is about 25 ppm

Table 2 Noise components of CryoSTM-TIAs

TIA type	Proposed in this work		Proposed in Ref.[3]	
C_A	8 pF		26 pF	
R_F	10 GΩ		1 GΩ	
f (kHz)	10	100	10	100
$\overline{e_A^2}$ $((nV)^2/Hz)$	0.5	0.14	0.5	0.14
Unit for the following terms is $(fA)^2/Hz$				
$\overline{i_A^2}$	0.17	2.9	0.8	20
$4k_BT/R_F$	0.02	0.02	0.2	0.2
$(2\pi f)^2 C C_{IJ} \overline{e_A^2}$	0.01	0.2	0.03	0.7
$(\frac{1}{R_J} + \frac{1}{R_F})^2 \overline{e_A^2}$	0.005	0.001	0.005	0.001
$\overline{i_{in}^2}$ as total	0.21	3.1	1.5	21

[20], the AC input signal voltage for STS measurements is capable as low as 30 R_J·fA, such as 0.3 μV for $R_J = 10$ MΩ, which is still 10 times higher than the inherent noise of the CryoSTM-TIA. Therefore, high-energy-resolution STS measurements can be achieved with this apparatus.

4 CryoSTM-TIA operating state adjustment and DC tunneling current measurement

For the proposed CryoSTM-TIA in Fig.1, CNRS-HEMTs $H1_1$, $H2_1$, $H1_2$, and $H2_2$ with the same performances should be selected as far as possible [11]. And, their gate-source voltage for the ideal operating point ($V_{ds} = 100$ mV and $I_{ds} = 1$ mA) should be $V_{gs} \leq -100$ mV. Gate P of $H2_1$ is constantly grounded.

Disconnect the Pre-Amp from the Post-Amp, and ground the input of the Pre-Amp, i.e. gate N of $H2_1$ is grounded. Adjust potentiometer R_{12} to $R_{L1} = R_{L2}$. Adjust the current generated by the constant-current source in dashed box (a2) of Fig.1 to $I_{sour} = 2$ mA. Adjust the resistance R_s to achieve the gate-source voltage V_{gs} of $H1_1$, $H2_1$, $H1_2$, and $H2_2$ for their operating points ($V_{ds} = -V_{gs}$ and $I_{ds} = 1$ mA). Since $V_{ds} \geq 100$ mV, all HEMTs operate in the saturation region, so their g_m and g_d are little changed comparing to those for the ideal operating point ($V_{ds} = 100$ mV and $I_{ds} = 1$ mA).

Cascade the Pre-Amp and Post-Amp to form the Macro-OPA. Then, the DC voltage V_{om} at the output of the Macro-OPA is called as the output offset voltage of the Macro-OPA. V_{om} is caused by the following factors: the common-mode DC voltages on the inputs of the Rear-OPA [13] in the Post-Amp, its input offset voltage, its input bias currents, and its input offset current. Usually, V_{om} is not 0. Adjusting R_{12}, it can be achieved that $V_{om} = 0$. $|a_{A0}|_{dB} \approx (g_m R_f)_{dB} \approx 95.6$ dB, which is consistent with the simulation result $|a_{A0}|_{dB} = 95.1$ dB in Fig.2(a). And, a_{A0} can be measured.

Connect gate N of $H1_1$ to the output of the Macro-OPA with the feedback resistor $R_F + R_k \approx R_F$, and then disconnect it from ground, therefore the TIA is formed. Connect the signal source circuit to the TIA, to form the CryoSTM-TIA. As the DC bias V_i is applied by BMS, the DC resistance of TJ is R, and

the potential at input N is V_N, and the output voltage of the CryoSTM-TIA is V_o. Obviously, $-a_{A0}V_N = V_o$, and $(V_i - V_N)/R = (V_N - V_o)/R_F$. The DC bias on TJ is $V = V_i - V_N$, and DC tunneling current $I = (V_i - V_N)/R$. I_s as an approximate value of the DC tunneling current I is

$$I_s = -V_o/R_F. \tag{4.1}$$

And, the relative error is obtianed as

$$Er = |I_s - I|/|I| = 1/(1 + a_{A0}),$$

and the DC bias on TJ is

$$V = V_i + V_o/a_{A0}. \tag{4.2}$$

With the measured V_o and a_{A0}, I_s and V can be obtained by Eqs.(4.1) and (4.2). Since $a_{A0} \approx 60,000$, $Er < 20$ ppm. And, as $R > 10^{-3}R_F$, $|V_o/a_{A0}| < |V|/60$, so $V \approx V_i$ with the error less than 2%. Therefore, with this apparatus, the DC tunneling current and the DC voltage on the tunnel junction can be obtained accurately.

5 Conclusions

In this work, a design of transimpedance amplifier (TIA) for cryogenic scanning tunneling microscope (CryoSTM) is presented. The TIA connected with the tip-sample component in CryoSTM is called as CryoSTM-TIA. A cascode-type configuration for the Pre-Amp of the CryoSTM-TIA is used to avoid Miller effect, so that the circuit is stable with gain of 10GΩ and bandwidth more than 100 kHz. And, its transient response time less than 10 μs. The apparatus inherent noise is only 0.21 $(\text{fA})^2/\text{Hz}$ at 10 kHz, and 3.1 $(\text{fA})^2/\text{Hz}$ at 100 kHz. With this apparatus, fast high-energy-resolution scanning tunneling spectra measurements can be performed for low conductivity materials, and their scanning tunneling shot noise spectra can be measured, even if the shot noise is very low.

Supplementary information. Supplemental file can be found on https://pan.baidu.com/s/1dmzt3-qost7JuOAXm-mkHA?pwd=1228.

Acknowledgments. This research did not receive any specific grant from funding agencies in the public, commercial, or not-for-profit sectors.

Declarations

The authors declare that they have no known competing financial interests or personal relationships that could have appeared to influence the work reported in this paper.

References

[1] Y. J. Song, A. F. Otte, V. Shvarts, Z. Y. Zhao, Y. Kuk, S. R. Blankenship, A. Band, F. M. Hess, and J. A. Stroscio, Invited Review Article: A 10 mK scanning probe microscopy facility, Rev. Sci. Instrum., 81 (2010) 121101.

[2] J. F. Ge, M. Ovadia, and J. E. Hoffman, Achieving low noise in scanning tunneling spectroscopy, Rev. Sci. Instrum., 90 (2019) 101401.

[3] Y. X. Liang, Low-noise large-bandwidth tansimpedance amplifier for measuring scanning tunneling shot noise spectra in cryogenic STM and its applications, Ultramicroscopy, 234, (2022) 13466.

[4] M. Carlà, L. Lanzi, E. Pallecchi, and G. Aloisi, Development of an ultralow current amplifier for scanning tunneling microscopy, Rev. Sci. Instrum.75 (2003) 497-501.

[5] C. C. Umbach and J. M. Blakely, Development of a sub-picoampere scanning tunneling microscope for oxide surfaces, Appl. surf. Sci. 175-176 (2001) 746-752.

[6] Q. F. Li, Q. Wang, Y. B. Hou, and Q. Y. Lu, 18/20 T high magnetic field scanning tunneling microscope with fully low voltage operability, high current resolution, and large scale searching ability, Rev. Sci. Instrum.83 (2012) 043706.

[7] Data sheet of FEMTO DE-DLPCA-200 Variable Gain Low noise Current Amplifier, https://www.femto.de/images/pdf-dokumente/de-dlpca-200.pdf; Data sheet of FEMTO DE-LCA-200-10G Ultra-Low-Noise Current Amplifier,https://www.femto.de/images/pdf-dokumente/de-lca-200-10g.pdf.

[8] F. Massee, Q. Dong, A. Cavanna, Y. Jin, and M. Aprili, Atomic scale shot-noise using cryogenic MHz circuitry, Rev. Sci. Instrum., 89 (2018) 093708.

[9] Y. X. Liang, Q. Dong, M. C. Cheng, U. Gennser, A. Cavanna, and Y. Jin, Insight into low frequency noise induced by gate leakage current in AlGaAsGaAs high electron mobility transistors at 4.2 K, Appl. Phys. Lett., 99 (2011) 113505.

[10] Y. Jin, Q. Dong, A. Cavanna, U. Gennser, L. Couraud, and C. Ulysse, Ultra-low noise HEMTs for deep cryogenic low-frequency and high-impedance readout electronics, 12th IEEE International Conference on Solid-State and Integrated Circuit Technology (ICSICT), Grenoble, France, 7-9 July 2014.

[11] Supplemental file. https://pan.baidu.com/s/1dmzt3-qost7JuOAXm-mkHA?pwd=1228

[12] Data sheet of BFT93 BJT, https://www.nxp.com.cn/docs/en/data-sheet/BFT93_CNV.pdf.

[13] Data sheet of THS4021 OPA, https://www.ti.com/lit/ds/symlink/ths4021.pdf.

[14] C. J. Chen, Introduction to Scanning Tunneling Microscopy, Oxford Univ. Press, Chapt.11, 1993.

[15] TINA-TI is SPICE-based analog simulation program produced by Texas Instruments Inc., https://www.ti.com/tool/TINA-TI.

[16] S. Franco, Design with Operational Amplifiers and Analog Integrated Circuits, McGraw-Hill Companies Inc., 2002.

[17] Keithley 2600B System SourceMeter SMU Instruments Datasheet, https://download.tek.com/datasheet/1KW-60906-1_Series_2600B_SMU_Datasheet_082821.pdf.

[18] A. van der Ziel, Noise in solid state devices and circuits, Wiley-Inter-Science, New York, (1986).

[19] Z. H. Qian, Study on noise models algorithms and matrix descriptions for integrated circuits, J Northeast Norm. Univ, 35 (2003) 41-46.

[20] SR830 Digital Lock-In Amplifier Datasheet, https://www.thinksrs.com/downloads/pdfs/catalog/SR810830c.pdf.